Design, construction and testing of a six-component force balance for the LNEC wind tunnel

Projeto, construção e ensaio de uma balança de forças para o túnel de vento do LNEC

Francisco R. B. M. Vaz[1] | **André C. Marta**[2] | **Fernando V. P. Oliveira**[1]

[1] LNEC – Laboratório Nacional de Engenharia Civil, Portugal, franciscobvaz@tecnico.ulisboa.pt, fvoliveira@lnec.pt

[2] IST – IDMEC, Instituto Superior Técnico, Universidade de Lisboa, Portugal, andre.marta@tecnico.ulisboa.pt

https://doi.org/10.82452/me20263706

abstract

Wind tunnel testing is still fundamental in the field of aerodynamics. At the National Laboratory for Civil Engineering (LNEC) a lot of studies are conducted on the wind tunnels where dedicated instrumentation is used for aerodynamic load measurements. On this work a new versatile 6-component aerodynamic balance recently developed according to the LNEC's requirements and considering the wind tunnel characteristics is presented. The concept was selected using the Analytic Hierarchy Process resulting in a Stewart platform configuration with six instrumented bars, enabling the measurement of three forces and three moments. The design was validated through singularity analyses, as well as analytical and numerical studies. Calibration followed a two-stage approach using a Weighted Least Squares method. The results demonstrate good accuracy and consistency instrument, which contributes to the improvement of the LNEC's wind tunnels' tools.

Keywords: Six-component aerodynamic balance, Experimental aerodynamics, Wind tunnel testing, Mechanical design, Calibration

resumo

Os ensaios em túnel de vento são ainda fundamentais na área da aerodinâmica. No Laboratório Nacional de Engenharia Civil (LNEC) são realizados estudos em túnel de vento que utilizam instrumentação dedicada na medição de cargas aerodinâmicas. Neste trabalho apresenta-se uma nova balança aerodinâmica de 6 componentes versátil desenvolvida recentemente seguindo os requisitos do LNEC e as características dos túneis de vento. O conceito foi selecionado através do Processo Hierárquico Analítico, resultando numa configuração em plataforma de Stewart com seis barras instrumentadas, permitindo medir três forças e três momentos. O projeto foi validado com análises de singularidades, assim como estudos analíticos e numéricos. A calibração seguiu uma abordagem em duas etapas, recorrendo a um Método Ponderado dos Mínimos Quadrados. Os resultados demonstram boa precisão e consistência do instrumento, o qual contribui para a melhoria das ferramentas existentes nos túneis de vento do LNEC.

Palavras-chave: Balança aerodinâmica de seis componentes, Aerodinâmica experimental, Ensaios em túnel de vento, Projeto mecânico, Calibração

1- INTRODUCTION

Wind tunnels are among the most important facilities for experimental aerodynamic testing, allowing controlled and repeatable study on scale models that are essential for validating the aerodynamic performance and detecting complex flow phenomena that simulations may overlook. At the Laboratório Nacional de Engenharia Civil (LNEC), wind tunnels are used for multiple purposes within civil engineering, namely testing the aerodynamic stability of bridges, analysing the behaviour of building structures and façade elements, study the conditions of comfort and pedestrian safety in open spaces, evaluating the vibrations induced on tower and chimney structures, as well as applications in aeronautical or automotive engineering. However, a versatile aerodynamic balance to measure aerodynamic forces and moments is not yet available. Commercial multi-component balances are often expensive or unsuited with specific requirements, motivating the development of a custom, adaptable, and cost-effective instrument.

Force balances can be classified into two broad categories: i) internal, usually placed inside the test model, requiring a custom design for each model; ii) and external, where the model is connected to an externally instrument using a support structure [1]. The platform balances represent one of the most common external force balance types, being the Stewart platform-based design highly regarded for modern experimental applications due to its versatility and capacity to measure the components. The generic design of a Stewart platform is constituted by two separate platforms connected by 6 bars with spherical joints on both ends. Among several configurations, the 6-6 type is the most generic, since it describes any platform with six vertices in each of the platforms [2]; see Figure 1 – a). As the bars are linearly independent, the resulting mechanism can accurately measure the six components of any applied load.

On this work are described the tasks performed to design, build, calibrate and test a Stewart platform force balance capable of measuring the three force and the three moment components, adaptable to different models and testing configurations, to be used on the LNEC's wind tunnels' testing facilities.

2- REQUIREMENTS AND CONCEPT SELECTION

To ensure that the force balance met the LNEC's needs, a set of requirements were defined taking into account various constraints and the expected testing scenarios. An Analytic Hierarchy Process (AHP) was used to select the optimal force balance concept. AHP is a multi-criteria decision analysis technique that enables systematic evaluation of different design alternatives by comparing them pairwise against weighted criteria, using both quantitative and qualitative measurements, ensuring a transparent selection process [3]. Six external force balance candidate designs were evaluated: platform, rotating platform, pyramidal, pyramidal platform and two innovative solutions. Twelve criteria covering both construction (criteria) and operational (criteria) aspects were chosen to evaluate the design, requiring a pairwise comparison of the criteria to define the respective weights. The final evaluation score revealed the platform force balance to be the most adequate option. The Stewart platform type 6-6 configuration was selected

to solve construction and joint challenges associated with simpler triangular configurations. Its geometry is fully defined by the side lengths of the top and bottom platforms, two coefficients controlling vertex placement, and the top platform height, a,b,α,β,h, respectively, as presented in Figure 1 – b), corresponding to the final adopted solution as depicted on Figure 1 – c).

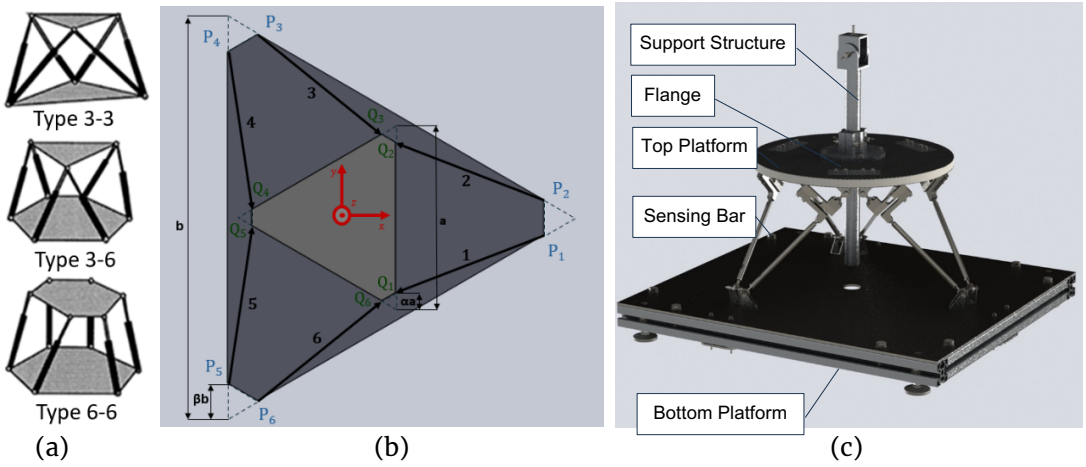

(a) (b) (c)

Fig. 1 | a) Stewart platforms' type; b) Force balance type 6-6 reference frame geometric dimensions and; c) adopted solution.

A standardized reference frame was defined according to international standards (ISO 1151/2), with the origin at the balance's attachment point, an upward pointing z-axis and, the x-axis aligned and pointing into the incoming flow, as shown in Figure 1-b). Wind tunnel specifications were also incorporated into the requirements, considering the Aeronautical Wind Tunnel (AWT) [4] and the Boundary Layer Wind Tunnel (BLWT) of LNEC. Five representative testing scenarios were analysed: a rectangular flat plate, a half wing model, a Formula Student car model, a suspension bridge section model, and a communications antenna. Aerodynamic coefficients and scaling laws were used to estimate the limiting forces and moments for each case. The results established the maximum load requirements as presented in Table 1. As the displacements significantly affect the applied aerodynamic loads, a limit of 2º was set for angular displacements and 10mm for linear displacements. Mechanical safety factors were defined using Pugsley's method [5], resulting in a general factor of 1.45, which was applied to the loads on the FEM simulations. Additional safety considerations were applied to the sensing bars to prevent yield and buckling, limiting the maximum axial force (500N) to 60% of the yield force and 70% of the critical buckling force. These requirements ensure that the force balance is both mechanically robust and capable of holding the test models at the set desired attitude across all operational scenarios.

Table 1 | Load cases for each testing scenario and corresponding load limits.

Load case	Fx [N]	Fy [N]	Fz [N]	Mx [N·m]	My [N·m]	Mz [N·m]
Flat Plate (AWT)	-493	0	0	0	-97	0
Flat Plate (BLWT)	-457	0	0	0	-192	0
Half Wing	-14	333	0	-133	-6	4
FS Car	-177	20	-550	-1	-15	-13
516 Arouca Bridge	-80	0	-8	0	1	0
Antenna	-0.20	0	0	0	-0.04	0
Limit Loads	-493	333	-550	-133	-192	-13

3- MEASUREMENT CHAIN

The measurement chain of the balance comprises the instrumentation, devices and computer system for measuring the axial forces acting on each sensing bar, as well as acquiring, processing and allowing data visualisation during wind tunnel experiments.

Beam loads cells were selected for their adaptability, metrological characteristics and, broad capacity range, while maintaining compatibility with other load cell alternatives. Each testing scenario was evaluated through a developed analytical model (described below) considering a minimum and maximum speed, used to estimate the axial forces prior each test. A 5kg and a 50kg beam load cells (HX711) were selected to cover the range of identified forces, where each type of load cell should be installed according to the expected load values from the model. This configuration provides full spectrum coverage with no effective discontinuity between the two ranges.

Data acquisition was implemented using National Instruments™ NI-9237 modules installed in a cDAQ-9178 chassis, capable of processing full Wheatstone bridges with high precision and signal conditioning. The wiring design emphasized modularity and electromagnetic interference prevention, employing DB15 connectors and shielded cables to enable quick sensor replacement and reliable signal transmission.

A dedicated LabVIEW™ User Interface was developed to manage acquisition parameters, display real-time readings, and register data for later post-processing. This integrated system provides accurate, flexible, and user-friendly instrumentation for the aerodynamic force balance, ensuring reliable performance for any user. Additional calibration interfaces were implemented to facilitate systematic load cell and balance calibration.

4- MECHANICAL DESIGN

The project was built upon a pre-existing prototype developed at LNEC, originally based on another force balance design [6]. The adopted concept already presented in Figure 1-c) comprises the following main components: i) bottom platform; ii) top platform; iii) flange; iv) 6 sensing bars, each one comprising one load cell and one adaptor, one connection rod and two rod end bearings; v) support structure assembly including one angle adjustment mechanism. The bottom platform is the support of the whole force balance and consists of a sheet steel base mounted on an extruded aluminium frame with four levelling feet, one in each corner, to allow a precise levelling of the balance. The top platform was designed to combine low mass with high stiffness and thus fabricated from a lightweight composite sandwich panel of carbon fibre reinforced polymer and foam core. The flange, which connects the support structure to the top platform, allows the support's position to be adjusted in height and lock the strut into position. The support structure was designed to provide height, angle of attack, and yaw adjustment while maintaining a minimal deformation under load. The sensing bars are the components that support the load between the two plates and allow

for the load measurement. These were designed to sustain purely axial loads without yielding or buckling, and thus all the designed parts for the sensing arms were manufactured using stainless steel (AISI 304), minimizing structural deformations while avoiding corrosion. A beam load cell (HX711) connected to a custom adaptor comprising a lever arm and a rod end connector, is installed on the top of the sensing bar – connection rod, allowing the beam load cell to measure the axial loads. Rod end bearings model SAKB-5-F and SALKB-5-F from SKF were fitted to each end of the bars to guarantee that the sensing bars only support axial loads. The connection rod diameter was selected to ensure compliance with the design requirements (yield and buckling), for an axial force of 500N.

An analytical model was established to describe the relationship between the applied aerodynamic loads and the corresponding axial forces in each of the six sensing bars. This model is defined by the main geometric parameters (a,b,α,β,h) which control the spatial configuration of the Stewart platform. The equation of the unit vectors from each of the bars V_i (vertices P and Q on the bottom and top platforms), as well as the forces and moments around the attachment point placed at a certain height d_s above the top platform function of the axial forces in each sensing bar r_i, are given by:

$$\overrightarrow{V_1} = \frac{1}{l}\left(\frac{a - b(2-3\beta)}{2\sqrt{3}}, \frac{a(2\alpha-1)+\beta b}{2}, h\right)$$
$$\overrightarrow{V_2} = \frac{1}{l}\left(\frac{a - b(2-3\beta)}{2\sqrt{3}}, \frac{a(1-2\alpha)-\beta b}{2}, h\right)$$
$$\overrightarrow{V_3} = \frac{1}{l}\left(\frac{a(1-3\alpha) - b(3\beta-1)}{2\sqrt{3}}, \frac{a(1-\alpha)-b(1-\beta)}{2}, h\right)$$
$$\overrightarrow{V_4} = \frac{1}{l}\left(\frac{a(3\alpha-2)+b}{2\sqrt{3}}, \frac{\alpha a - b(1-2\beta)}{2}, h\right)$$
$$\overrightarrow{V_5} = \frac{1}{l}\left(\frac{a(3\alpha-2)+b}{2\sqrt{3}}, \frac{-\alpha a - b(2\beta-1)}{2}, h\right)$$
$$\overrightarrow{V_6} = \frac{1}{l}\left(\frac{a(1-3\alpha) - b(3\beta-1)}{2\sqrt{3}}, \frac{a(\alpha-1)-b(\beta-1)}{2}, h\right)$$

l – distance between points

$$F_x = -\sum_{i=1}^{6} r_i \cdot V_{i_x}$$
$$F_y = -\sum_{i=1}^{6} r_i \cdot V_{i_y}$$
$$F_z = -\sum_{i=1}^{6} r_i \cdot V_{i_z}$$
$$M_x = \sum_{i=1}^{6}\left(-r_i \cdot V_{i_z} \cdot Q_{i_y}\right) + \sum_{i=1}^{6}\left(-r_i \cdot V_{i_y} \cdot d_s\right)$$
$$M_y = \sum_{i=1}^{6}\left(r_i \cdot V_{i_z} \cdot Q_{i_x}\right) + \sum_{i=1}^{6}\left(r_i \cdot V_{i_x} \cdot d_s\right)$$
$$M_z = \sum_{i=1}^{6}\left(r_i \cdot V_{i_x} \cdot Q_{i_y}\right) + \sum_{i=1}^{6}\left(-r_i \cdot V_{i_y} \cdot Q_{i_x}\right) \quad (1)$$

The design variables had to be carefully chosen to avoid singularities, which are conditions where the force balance is unable to support one or more components of the load [7]. To assess the quality of the design, a quality index λ was defined as:

$$\lambda = \frac{|J|}{|J|_m}$$
$$J = [\widehat{S_1} \quad -\widehat{S_2} \quad \widehat{S_3} \quad -\widehat{S_4} \quad \widehat{S_5} \quad -\widehat{S_6}] \quad (2)$$
$$\widehat{S_i} = \left[x_{Q_i} - x_{P_i},\ y_{Q_i} - y_{P_i},\ z_{Q_i} - z_{P_i},\ y_{P_i}z_{Q_i} - y_{Q_i}z_{P_i},\ x_{P_i}z_{Q_i} - x_{Q_i}z_{P_i},\ x_{P_i}y_{Q_i} - x_{Q_i}y_{P_i}\right]^T$$

where: $|J|$ and $|J|_m$ represent the determinant of the Jacobian matrix of a specific design and of the optimal design respectively and, $\widehat{S_i}$ represents the Plucker coordinates of the i_{th} bar. A design with a quality index of 1 represents an optimal design, whereas a design with a quality index of 0 is a design with singularities. Having the platforms geometry defined in advance, only the height h could be adjusted, and setting it to h=205mm, an almost optimal design is achieved, i.e. λ=0.997.

An FEM analysis was performed on the complete assembly under the defined load cases to ensure compliance with the requirements. The simulations were performed using parabolic tetrahedral elements with a refined curvature-based mesh on stress concentration regions, namely on the rod end bearings components. A mesh convergence study was performed ensuring a balance between accuracy and computational cost, resulting in a final mesh containing approximately 1.25×10^5 elements. The displacement values at the attachment point versus the number of elements is shown in Figure 2-a). The results confirmed that the design met all displacement and stiffness requirements. The most demanding case corresponded to the flat plate load configuration, whose displacement plot is shown in Figure 2-b), which resulted in a maximum linear displacement of 8.12mm and an angular displacement of 1.73º, both within the prescribed limits.

These results validate the adequacy of the design and confirmed the overall mechanical robustness of the force balance considering the specified requirements.

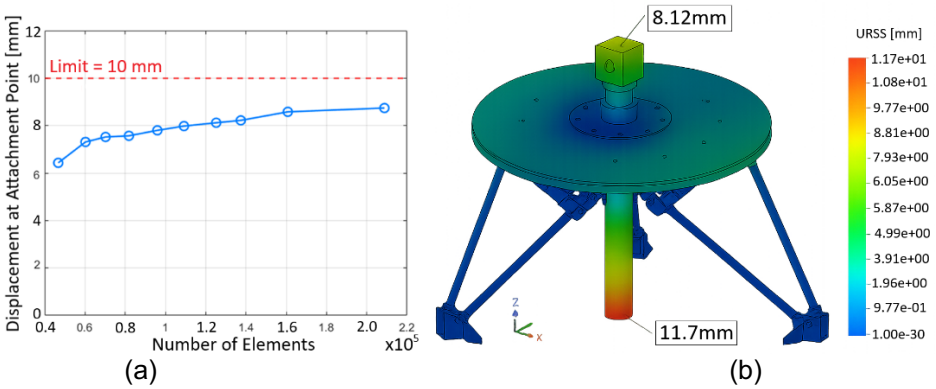

(a) (b)

Fig. 2 | FEM results: a) Linear displacements convergence study; b) FEM Linear displacements plot.

5- CALIBRATION

The developed force balance (Figure 3-a)) calibration process was performed in two main steps: individual load cell calibration and global force balance calibration.

(a) (b) (c)

Fig. 3 | a) Force Balance; b) Load cell calibration setup; c) Force balance calibration setup.

Each load cell was first calibrated using a dedicated calibration jig as shown in Figure 3-b) and different masses traceable to reference standards were used to apply the steps test loads. The apparatus consisted of a base plate and a pulley system that allowed the application of both tensile and compressive loads in a controlled and purely axial manner. The calibration procedure involved 21 incremental load steps, from -50N to +50N, performed in three complete cycles to evaluate the sensor repeatability and reversibility. The acquired data was used to establish a mathematical model between output voltage and axial load, evaluate the measurement uncertainty following the recommendations of international standards [9]. Seven main sources of uncertainty were considered: slope, intercept, linearity, reversibility, repeatability, output voltage, and excitation voltage. The uncertainty balance of the load cell with the largest uncertainty is presented in Table 2. The expanded uncertainties (95% confidence) were found to be below 0.4% of full scale for all six load cells, and the results proving to be consistent across each repetition.

Table 2 | Uncertainty balance for a single load cell.

Sources of uncertainty	DOF	Contribution
Slope	2	0.030 N (9.5%)
Intercept	2	0.017 N (3.0%)
Input Voltage	50	0.056 N (33.2%)
Max Output Voltage	50	0.056 N (33.8%)
Linearity	2	0.042 N (18.6%)
Reversibility	11	0.012 N (1.5%)
Repeatability	23	0.005 N (0.3%)
Standard Load	50	0.001 N (0.0%)
r(m,b)	22	0.002 N (0.0%)
Combined Uncertainty		0.097 N (100.0%)
Effective DoF		37
Expansion Factor		2.03
Expanded Uncertainty (95%)		0.196 N (0.39 %FS)

The second calibration stage focused on the complete six-component force balance, to establish a relationship between the six bar outputs to the aerodynamic loads applied at the model's attachment point. The process consists in applying N known loads to the force balance, creating N calibration points, whose values are fitted to a second order polynomial model, that accounts for both direct and cross-coupling effects between the sensing bars, which improves the accuracy over a first order approach [10, 11]:

$$F = CR + \epsilon,$$
$$R = [r_1 \quad r_2 \quad \cdots \quad r_6 \quad r_1^2 \quad r_1 r_2 \quad \cdots \quad r_6^2] \tag{3}$$

where: $F=[F_x, F_y, F_z, M_x, M_y, M_z]^T$ is the vector of aerodynamic forces and moments, r_i represents the axial load on each bar, C is the matrix of parameters that results from the calibration process, and ϵ is the model error (vector of calibration errors).

An experimental calibration setup consisting of a dedicated jig designed to allow the application of pure forces, moments as well as combined loads through steel cables, pulleys, and a steel arm connected at the attachment point, was developed as shown in Figure 3-c). A total of 24 load cases containing 178 calibration points were considered representative of the aerodynamic loading conditions over the entire measurement range of the force balance. Each point was repeated three times to reduce statistical variability. The calibration coefficients were obtained using the Weighted Least Squares Method including the variability and uncertainty of each test [10, 11]. Following the described calibration process (in detail on [10, 11]), a final calibration 6×27 matrix C was achieved. The uncertainty of the calibrated model can be assessed by propagating the uncertainties from the load measurements in each bar and the uncertainties of the calibrated model itself [11]. An example for the load case [F_x(-), F_z(-) M_y(+)] is presented in Table 3, where it is observed an increase of the uncertainty values with the load magnitude since the uncertainty is accounting for the measurement error and the decoupling between different load components.

Table 3 | Fitted loads F_i & M_i and uncertainties u for the load case [F_x(-), F_z(-) M_y(+)].

Fx [N]	**uFx** [N]	**Fy** [N]	**uFy** [N]	**Fz** [N]	**uFz** [N]	**Mx** [N·m]	**uMx** [N·m]	**My** [N·m]	**uMy** [N·m]	**Mz** [N·m]	**uMz** [N·m]
0.00	0.11	0.00	0.12	0.00	0.16	0.00	0.04	0.00	0.04	0.00	0.02
-0.86	0.11	-0.01	0.12	-1.00	0.17	0.00	0.04	0.16	0.04	0.00	0.02
-11.53	0.13	0.09	0.11	-11.57	0.28	0.01	0.07	1.65	0.07	-0.07	0.06
-21.77	0.15	0.17	0.12	-21.88	0.47	0.02	0.09	3.13	0.10	-0.10	0.08
-31.56	0.17	0.25	0.14	-31.82	0.67	0.01	0.12	4.64	0.12	-0.11	0.10
-41.15	0.26	0.19	0.25	-51.57	1.20	-0.01	0.20	7.63	0.22	0.03	0.19
-49.65	0.45	-0.01	0.45	-70.35	1.78	-0.05	0.38	10.74	0.41	0.32	0.37

6- TESTING

Three models were tested to comprehensively assess the accuracy, reliability and operational behaviour of the force balance: two rectangular flat plates (a short one with 100.7×150.7 mm and, a larger one with twice dimensions); and a flat disk (100 mm diameter). All the tests were performed at LNEC Aerodynamic Wind Tunnel, covering 12 measurement points in a range of velocities between 5m/s to 30m/s, in both ascending and descending directions to assess linearity and reversibility. The models were fixed at the centroid to the attachment point to ensure it only generates drag and no additional load. A fairing was added around the arm that supports the plates to mitigate any potential added drag on the arm.

The measured drag forces exhibited the expected quadratic dependence on airspeed, confirming the correct functioning of the balance. The obtained coefficients of determination r^2 are higher than 0.9999999, evidencing a good fit between the measured drag force and wind velocity. Analysing the calculated drag coefficients C_d function of the Reynolds number

R_e, as shown in Figure 4, it is observed that the values are almost constant when the air speed was increasing, as is expected for the range of Reynolds numbers R_e tested. However, under decreasing velocities the drag coefficient reduces as R_e decreases, reaching significant differences at the lowest air speeds. This is observed on all tests in general, which was associated to a systematic error on the force balance. This point was analysed in detail by conducting multiple consecutive runs on the larger flat plate model and it was observed that the error was only present on the first run, which could be explained by friction in the rod end bearings. To minimize this effect it is recommended to run up to an air speed slightly higher than the maximum intended value before the test. Regarding the measured drag coefficients, it is observed that the average value calculated for the rectangular flat plate C_D=1.45 is aligned with the values found on the literature. For example, 3D finite rectangular flat plates have values that fall between 1.1 and 1.3 [12, 13, 14], but these values can change depending on multiple factors, such as aspect ratio, roughness, blockage ratio, among others. However, as the support structure is placed aft of the model, the interference with the airflow can cause a change in the base pressure behind, causing an increase in drag, as is demonstrated by several experimental tests [15, 16]. Despite this, the results proved to be consistent, highlighting the accurate and reliable performance of the force balance.

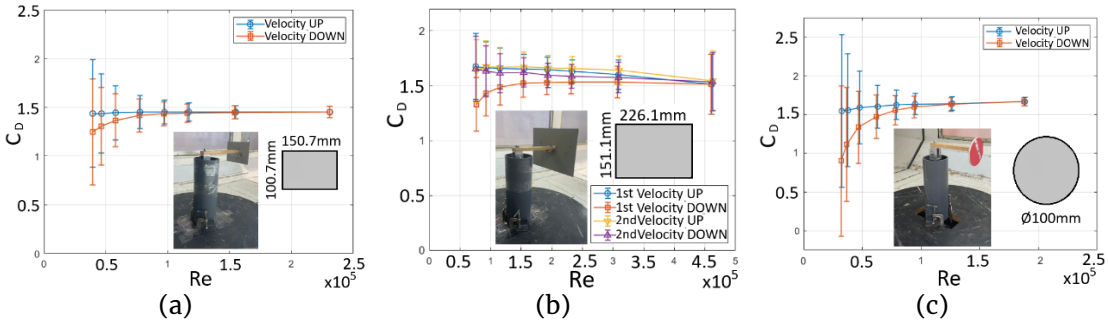

Fig. 4 | Drag coefficient: a) short rectangular flat plate; b) large rectangular flat plate; c) circular flat plate.

7- CONCLUSIONS

On this work was presented the design, development, and calibration of a six-component aerodynamic force balance for the LNEC's wind tunnels. The final design is based on the Stewart platform concept which provides structural efficiency and measurement decoupling. Finite element analyses confirmed the balance's stiffness and reliability under the defined operational loads, while efforts were made to minimize component mass and manufacturing cost. Six commercial beam load cells were integrated as sensing elements, chosen for their precision and flexibility, whose metrological characterisation performed showed good results (expanded uncertainties below 0.4% of full scale). The whole force balance calibration was conducted using a custom jig that allowed the application of known loads. The adopted model was a second-order polynomial fitted to the data using the Weighted Least Squares Method, capturing both direct and cross-coupling effects and accounting for sensor uncertainty. Experimental validation involved three different standard models tested at

known wind velocities. The results demonstrated consistent and accurate measurements across the full operational range, with deviations mainly attributed to test setup limitations. In conclusion, the developed balance successfully met all design and performance requirements and provides LNEC with an effective and adaptable tool for precise aerodynamic load measurement, significantly improving the experimental and research capabilities. Finally, as a complement of this paper the MSc thesis of the same author [17] may be consulted for further clarification of any specific detail.

REFERENCES

1. Barlow, J. B., Rae, W. H., Pope, A. Low Speed Wind Tunnel Testing. John Wiley&Sons, 3rd edition, 1999. ISBN 9780471557746
2. Dasgupta, B., Mruthyunjaya, T . The stewart platform manipulator: A review. Mechanism and Machine Theory, 35(1):15–40, January 2000. doi:10.1016/S0094-114X(99)00006-3.
3. Vaidya, O. S., Kumar, S. Analytic hierarchy process: An overview of applications. European Journal of Operational Research, 169(1):1–29, February 2006. doi:10.1016/j.ejor.2004.04.028.
4. Borges, A. R. J. O túnel aerodinâmico do Laboratório Nacional de Engenharia Civil., volume M 319 of Memórias. LNEC, 1969.
5. Musto, J. C. The safety factor: Case studies in engineering judgment. International Journal of Mechanical Engineering Education, 38(4):286–296, 2010.

   doi:10.7227/IJMEE.38.4.2.
6. Ferreira, M. Design of a Six-Component External Wind Tunnel Balance. MSc Thesis in Mechanical Engineering, Instituto Superior Técnico, Lisboa, Portugal, July 2015.
7. Lee, J. Investigation of quality indices of in-parallel platform manipulators and development of Web-based analysis tool. University of Florida, 2000.
8. Budynas, R. G., Nisbett, J. K. Shigley's Mechanical Engineering Design. McGraw-Hill Series in Mechanical Engineering. McGraw-Hill Education, New York, NY, USA, 9th edition, 2011. ISBN 978-0-07-352928-8.
9. BIPM, IEC, IFCC, ILAC, ISO, IUPAC, IUPAP, and OIML. Evaluation of measurement data — Guide to the expression of uncertainty in measurement. Joint Committee for Guides in Metrology (JCGM), JCGM 100:2008, 2008.
10. Reis, M., Castro, R., Mello, O. Calibration uncertainty estimation of a strain-gage external balance. Measurement, 46(1):24–33, 2013. doi:10.1016/j.measurement.2012.07.019.
11. Reis, M. L. C. C., Mello, O. A. F., Uyeno, S. Calibration uncertainty of an external six-component wind tunnel balance. In Proceedings of the 33rd AIAA Fluid Dynamics Conference and Exhibit.

American Institute of Aeronautics and Astronautics (AIAA), Orlando, FL, USA, June 2003. doi:10.2514/6.2003-3884.

12. Fail, R., Lawford, J., Eyre, R. Low-speed experiments on the wake characteristics of flat plates normal to an air stream. Aeronautical Research Council Reports & Memoranda, 3120, 1957.

13. NASA Glenn Research Center. Shape effects on drag — drag coefficient. Accessed: October 2025.

14. Hoerner, S. F. Fluid-Dynamic Drag: Theoretical, Experimental and Statistical Information. Hoerner Fluid Dynamics, Brick Town, New Jersey, USA, 2nd edition, 1965. ISBN 9991194444. First published 1958 (1st ed.), Library of Congress Catalog Card Number 64-19666.

15. Powers, S. G., Huffman, J. K., Charles, J. K., Fox., H. Flight and wind-tunnel measurements showing base drag reduction provided by a trailing disk for high reynolds number turbulent flow for subsonic and transonic mach numbers. NASA Technical Publication (NASA-TP-2638) 2638, National Aeronautics and Space Administration, Scientific and Technical Information Branch, Edwards, California / Hampton, Virginia, USA, November 1986. Dryden Flight Research Facility, Ames Research Center; Langley Research Center. doi:10.2514/6.2003-3884.

16. Hetherington, B.. Interference of Supports Used for Ground Vehicle Wind Tunnel Testing. Ph.D. thesis, Durham Thesis, Durham University, 2006.

17. Vaz, Francisco. Design, Construction and Testing of a Six-Component Force Balance for the LNEC Wind Tunnel. MSc Thesis in Aerospace Engineering, Instituto Superior Técnico, Lisboa, Portugal, December 2025.